TOWARDS AUTOMATED DIAGNOSTIC EVALUATION OF RETINA IMAGES

H. Niemann[4], R. Chrastek[4], T. Hothorn[3], B. Lausen[3], L. Kubečka[2], J. Jan[2], G. Michelson[1]

[1] Department of Ophthalmology and University Eye Hospital, Universität Erlangen-Nürnberg, Schwabachanlage 6, 91054 Erlangen, Germany, georg.michelson@rzmail.uni-erlangen.de
[2] Department of Biomedical Engineering, Faculty of Electrical Engineering and Communication, Brno University of Technology (BUT), Kolejni 2906/4, 61200 Brno, Czech Republic xkubec01@stud.feec.vutbr.cz, jan@feec.vutbr.cz
[3] Department of Medical Informatics, Biometrics, and Epidemiology, Universität Erlangen-Nürnberg, Waldstr. 6, 91054 Erlangen, Germany, {thorsten.hothorn, berthold.lausen}@rzmail.uni-erlangen.de
[4] Chair for Pattern Recognition (Informatik 5), Universität Erlangen-Nürnberg, Martenstr. 3, 91058 Erlangen, Germany {niemann, chrastek}@informatik.uni-erlangen.de

In this paper we describe the automatic segmentation of the optic nerve head (ONH) with the long-term goal to diagnose automatically early stages of glaucoma. The images are average images obtained from a scanning laser ophthalmoscope (SLO). The segmentation consists of the main steps of finding a region of interest containing the ONH, constraining the search space for final segmentation, and computing the fine segmentation by an active contour model. The agreement of 'true positive pixels', i.e. pixels attributed to the ONH by both manual and automatic segmentation, is very good. The classification results from three different classifiers using manual or automatic segmentation still show an advantage of manual segmentation. One means to further improve the automatic segmentation is to use information from a SLO as well as from a fundus camera.

Introduction

Among the promising areas for medical image processing is the (early) automatic diagnosis of frequently occurring and severe diseases. It offers the potential to reduce the time for diagnosis or to increase the number of persons screened, to establish standardized, reproducible, and economic procedures, and in the long run to reduce the costs of treatment and to reduce errors if more and more cases are being evaluated and documented resulting in improved algorithms. Two frequent and severe diseases are glaucoma - the second most common cause of blindness in developed countries [11, 15] - and stroke - the third most frequent cause of death in Germany. Glaucoma basically destroys the optic nerve head (ONH), an effect visible in images of the retina which are available from different imaging devices. We concentrate in our work on the so called "open angle glaucoma". A stroke is a sudden blocking (or also a bleeding) of a vessel (artery or vein) in the brain. A hypothesis is that the risk of blocking may be estimated from the vessels visible in the retina.

Types of Images

Images of the retina may be obtained by a fundus camera (FC), a scanning laser ophthalmoscope (SLO), or a scanning laser DOPPLER flowmetry device (SLDF). The SLO became a widely used imaging device for measuring the ONH [13, 10, 3], and we use images obtained with a "Heidelberg Retina Tomograph (HRT)" [4]. It records a series of

images at different depths from which also an average image is computed as shown in Fig. 1. In addition FC images are available with two examples given in Fig. 2.Work based on SLDF images is reported in [14].

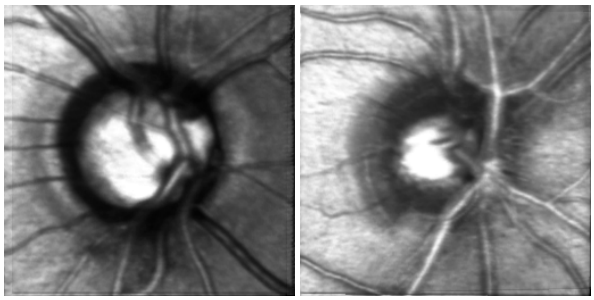

glaucoma normal

Fig. 1. Two examples of HRT average images.

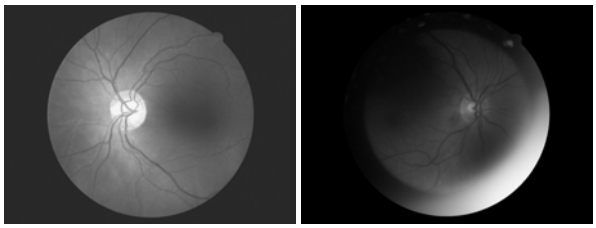

left eye, “good” image right eye, “bad” image

Fig. 2. Two examples of FC images.

Segmentation of the Optic Nerve Head

Diagnosis of glaucoma using the HRT images is based on features (parameters) which are computed by the HRT software after manual or automatic outlining of the contour of the optic nerve head (ONH). Examples of features are the disk area, the area of cup and rim, the volume of cup and rim, the mean and maximum cup depth, and a measure for the three-dimensional shape of the cup. The reproducibility of ONH borders was investigated in [7, 12] and showed the desirability of automatic and reproducible approaches.

An overview of the processing steps to segment the optic nerve head (ONH) is given in Fig. 3. The four main steps are preprocessing to correct non-uniform illumination, the determination of a region of interest containing the ONH, the constraining of the search space for refining the ONH contour, and finally the computation of the ONH contour using an active contour model.

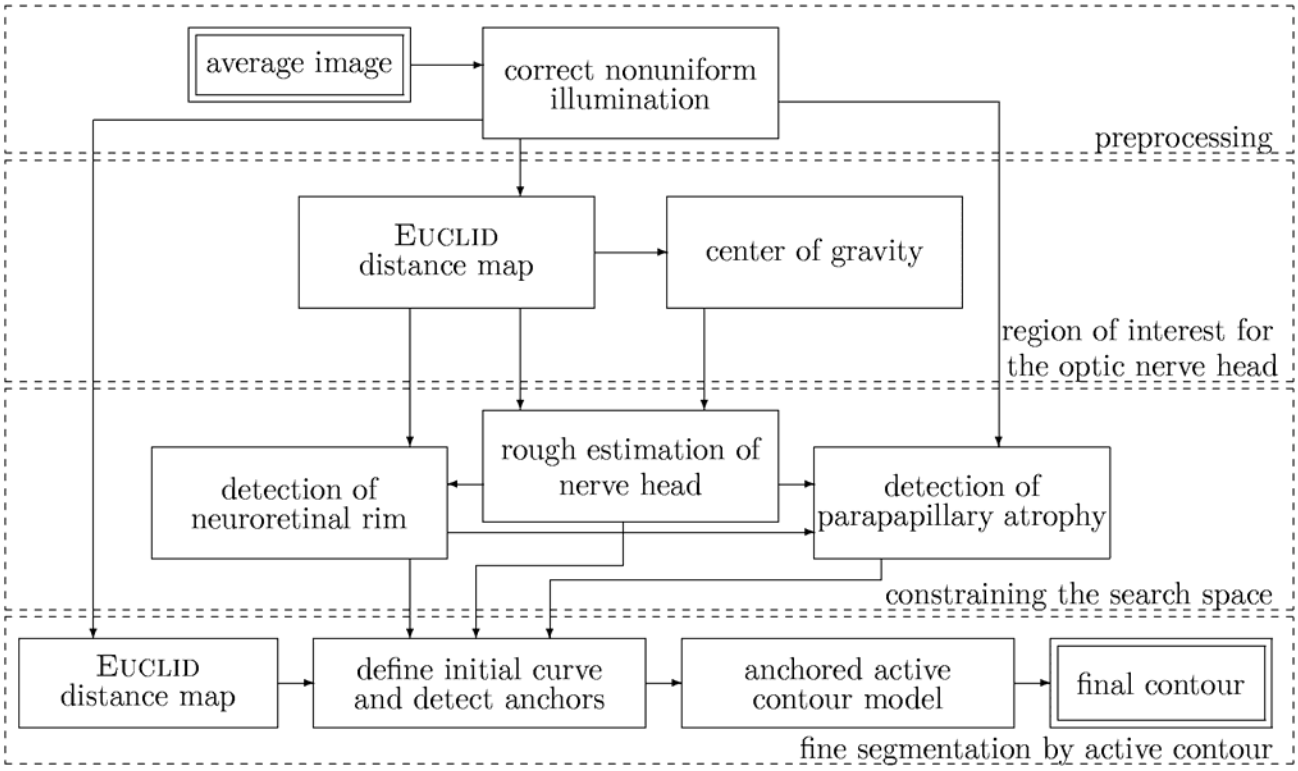

Fig. 3. The processing steps to automatically segment the ONH

Preprocessing

The goal of preprocesing is to correct for non-uniform illumination. Let the input image be denoted by $f_{ij}^{(in)}, i = 0, 1, \cdots, M_y,\ j = 0, 1, \cdots, M_x$.

To estimate nonuniform illumination a median filtering with a mask of size 31×31 is performed, which is large with respect to the maximal vessel diameter (about 10 pixels), but small with respect to the ONH (about 160 pixels). The result of median filtering is an image $f_{ij}^{(med)}$. We compute correction coefficients

$$r_{ij} = \frac{\max_{i,j}\left(f_{ij}^{(med)}\right)}{f_{ij}^{(med)}}$$

and adjust the difference image by the correction coefficients to get

$$f_{ij}^{(adj)} = \left(f_{ij}^{(in)} - f_{ij}^{(med)}\right) r_{ij} + c\,.$$

The constant c is chosen to make the mean value of $f_{ij}^{(adj)}$ approximately equal to 128.

The final corrected output image (Fig. 4) is computed from

$$f_{ij}^{(corr)} = \begin{cases} 0 & : \ f_{ij}^{(adj)} \le 0 \\ 255 & : \ f_{ij}^{(adj)} \ge 255 \\ f_{ij}^{(adj)} & : \ \text{else} \end{cases}$$

In addition, to eliminate border effects, the image borders are removed.

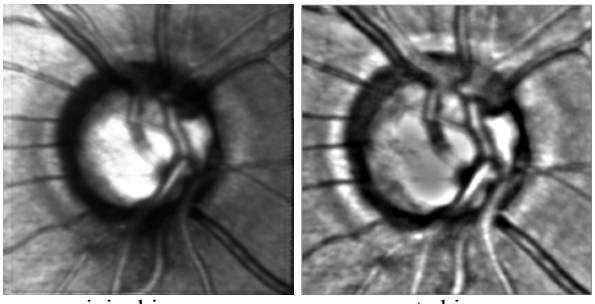

original image corrected image

Fig. 4. Correction of nonuniform illumination.

Region of Interest for the ONH

The goal of this step is to find a region smaller than the original image and containing the ONH. The basic approach is to find the dark regions of the ONH, but remove blood vessels and noise. Hence, the image is binarized by a threshold $\theta_1 = \mu - 0.25\sigma$, where μ and σ are the mean value and standard deviation of the grey values of the corrected image $f_{ij}^{(corr)}$. Next we compute an EUCLID distance map (EDM) which assigns to each pixel its distance from the nearest boundary point and threshold the EDM by θ_2 to remove vessels. Since the maximal vessel diameter is about 10 pixels, $\theta_2 = 6$ is selected. The rough position of the ONH is taken to be the center of gravity of the remaining pixels and the size of the ROI is set to for a $20° \times 20°$ field of view in the HRT image.

Constraining the Search Space

The goal of this step is to provide a good *initialization* for the subsequent fine segmentation of the ONH which is done by an active contour model. This is done by fitting a circle to the ONH with algebraic curve fitting (Fig. 5), by fitting a circle to the neuroretinal rim (NRR) with the HOUGH transform (Fig. 5), and by fitting a circle to the parapapillary atrophy (PPA) (Fig. 6). The contours of ONH and NRR should coincide, but different approaches are used to improve the result. Only the circle fitting to the ONH is outlined briefly. We start from the EDM of the previous step and binarize it by $\theta_3 = 2$ to filter out artifacts from the background, but preserve relevant structures. A circle is fitted to points on the perimeter of the thresholded EDM which minimizes the algebraic distance (least square sense), and then the geometric distance is optimized by GAUSS-NEWTON iteration. The result is improved by shifting the circle to the point of maximum correlation between the filled circle and the potential nerve head region.

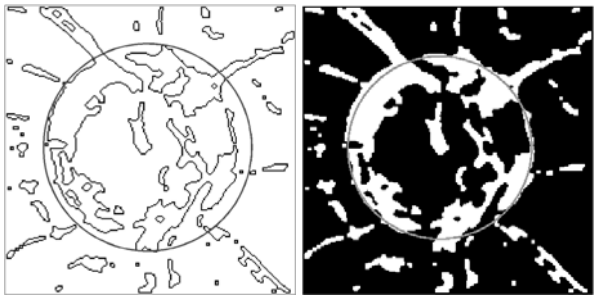

Fig. 5. Constraining the search space by circle fitting procedure (*left*) and by NRR detected with the Hough transform (*right*).

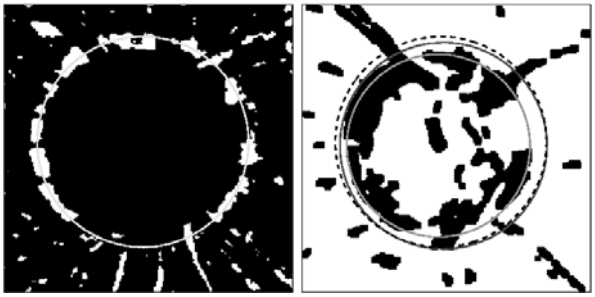

Fig. 6. Constraining the search space by PPA detected by the Hough transform (*left*). All constraing factors together (*right*).

Active Contour

The goal of this step is to improve the result for the ONH from the last step by using an active contour model. We start from the illumination corrected intensity image and threshold it by $\theta_4 = \mu - 0.5\sigma$. Another EDM is computed and thresholded by $\theta_5 = 2$ to obtain potential regions of the ONH. Potential anchor points of the active contour are defined as change from foreground to background in radial direction. The potential anchor points are refined to *suitable* anchor points (Fig. 7) by a rule-based approach which distinguishes the cases where the PPA is detected or not detected. If the PPA is detected and its approximating circle intersects with the circle approximating the NRR in 95%, then the PPA circle is the outer limit for anchor points. If the PPA is *not* detected and the ONH is large or with good identifiable NRR, then the circle determined by the fitting procedure ─ but without correction by correlation ─ is used as outer limit of anchor points. If the PPA is *not* detected and the ONH is large or with good identifiable NRR, then the circle obtained from the fitting procedure is used as outer limit of anchor points.

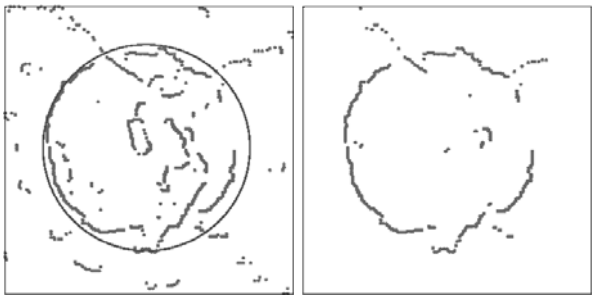

Fig. 7. Potential anchors (*left*) and suitable anchors (*right*).

A circle is used to initialize the active contour (Fig. 8). The final contour is found by balancing two types of forces: internal and external. Internal forces keep the contour shape smooth under external loads in the tangential and normal direction. External forces are derived from image data and attract the contour to pixels with some desirable features [2]. In our case internal force controls the elasticity and rigidity of the initial curve. For the computation of external forces we adopted a modified model of active contours ─ anchored snakes. This method consists of directly searching for the best points in the image to which the initial curve should be attracted. For each contour point a unique anchor, i.e., a unique source of the external force is detected (Fig. 8). A spring connection is then established between the point and the anchor (Fig. 8). The final contour obtained by the least square approach [9] can be seen on Fig. 9.

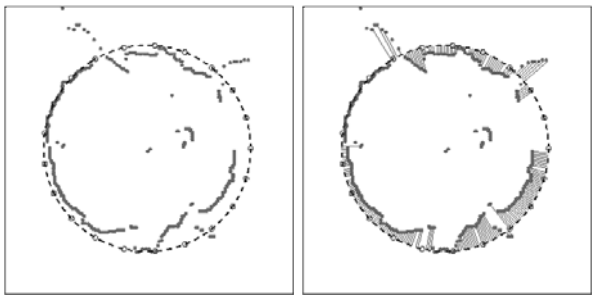

Fig. 8. Initialization of the active contour (*left*) and spring connections between the initial curve and the anchors (*right*).

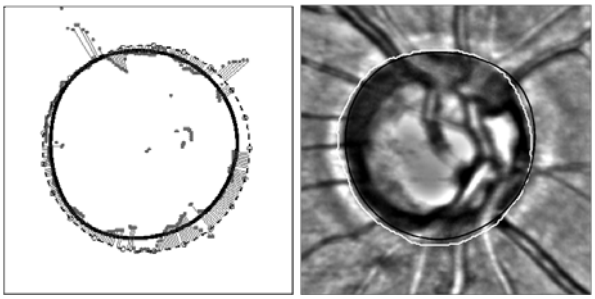

Fig. 9. The final contour. Black line: automatic segmentation; white line: segmentation by a medical expert.

Results

Examples comparing manual and automatic segmentation of the ONH are given in Fig. 10 and Fig. 11, respectively. We denote as "true positive pixels" the number of pixels which are attributed to the ONH both by manual and by automatic segmentation. On a sample of 159 images containing normal and glaucoma cases the average percentage of true positive pixels is about 91%.

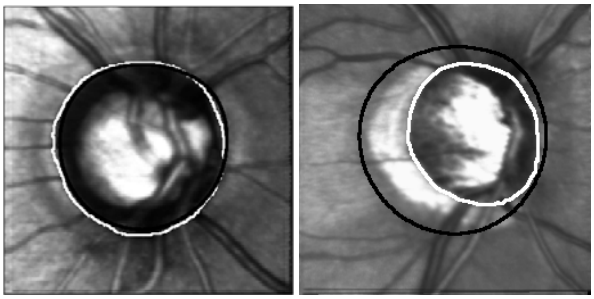

Fig. 10. Eye with glaucoma: an example of a good (*left*) and a bad (*right*) agreement between manual (*white*) and automatic (*black*) segmentation of the ONH contour.

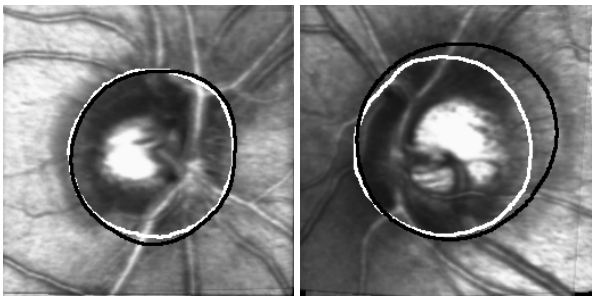

Fig. 11. Normal eye: an example of a good (*left*) and a bad (*right*) agreement between manual (*white*) and automatic (*black*) segmentation of the ONH contour.

More important than the segmentation is the classification of glaucoma and normal cases. Once the ONH boundary is available, classification is presently done by features (parameters) computed from the HRT software; different classifiers can be used. Using features based on *manually* outlined ONH contours an LDA classifier achieves 26.8% error rate, a bagging tree classifier [5] 13.4%. Using features based on *automatically* outlined ONH contours an LDA classifier achieves 27.7% error rate, a bagging tree classifier 22.2%.

Fusion of Segmentation Results

Fundus camera images are used to compute the arterio-venous ratio (AVR) for the assessment of stroke risk. The AVR is computed according to [6] and needs, among others, the segmentation of the ONH in FC images. Details of this segmentation are given in [1]. From this work a segmentation of the ONH using an imaging modality which is different from the HRT images is available. An obvious idea is to use segmentation results from both HRT and FC images to improve the overall accuracy of segmentation.

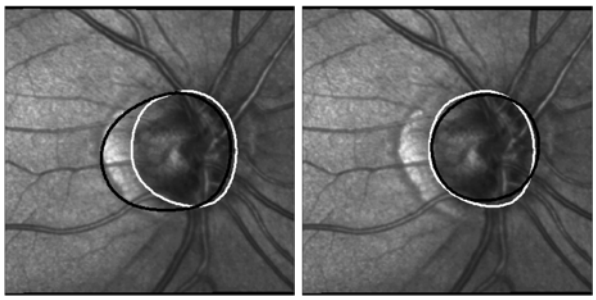

Fig. 12. Improvement of segmentation by fusion of segmentation results from HRT and FC images; false automatic monomodal segmentation on HRT image (*left*); improved multimodal segmentation (*right*). Black line: automatic segmentation; white line: segmentation by a medical expert.

At first, both images are registered using the mutual information criterion and controlled random search for optimization of this criterion [8]. This registration is successful in about 94% of cases, evaluated on 174 images. The criterion for correctness was the agreement of vessels in the registered images. Then the search area for

the optimization of the active contour is constrained by the segmentation result obtained from FC images. Fig. 12 shows an example where this approach resulted in a significant improvement of the segmentation result. The impact of the fusion of segmentation results from the two modalities on the reliability of glaucoma classification is subject to forthcoming work.

Outlook and Conclusion

The classification results show that manual segmentation still gives better classification results than automatic segmentation. A further improvement of automatic segmentation is expected if it is performed both on fundus and on scanning laser images and if the results of both segmentations are fused.

Acknowledgment: The work reported here was supported by the German Research Foundation (DFG), SFB 539, TP A4, the grant of the Grant Agency of Czech Republic 102/02/0890 and the bilateral grant KONTAKT CZE 01/031. Only the authors are responsible for the content of this paper.

References

1. R. Chrástek, M. Wolf, K. Donath, H. Niemann, and G. Michelson. Automated calculation of retinal arteriovenous ratio for detection and monitoring of cerebrovascular disease based on assessment of morphological changes of retinal vascular system. In Proceedings of IAPR Workshop on Machine Vision Applications, pages 240-243, Nara, Japan 2002. (ISBN 4-901122-02-9).
2. L. D. Cohen and I. Cohen. Finite element methods for active contour models and balloons for 2-D and 3-D images. IEEE Transactions on Pattern Analysis and Machine Intelligence, 15:1131-1147, 1993.
3. M. J. Greaney, D. C. Hoffmann, D. F. Garway-Heath, M. Nakla, A. L. Coleman, and J. Caprioli. Comparison of optic nerve imaging methods to distinguish normal eyes from those with glaucoma. Investigative Ophthalmology & Visual Science, 43:140-145, 2002.
4. Heidelberg Engineering GmbH. Quantitative Three-Dimensional Imaging of the Posterior Segment with the Heidelberg Retina Tomograph.http://www.heidelbergengineering .de/tut/hrt/hrt-tutorial.html, 1997.
5. T. Hothorn and B. Lausen. Bagging tree classifiers for laser scanning images: Data- and simulation-based strategy. Artificial Intelligence in Medicine, 27:65-79, 2003.
6. L. D. Hubbard, R. J. Brothers, W. N. King, L. X. Clegg, R. Klein, L. S. Cooper, A. R. Sharrett, M. D. Davis, and J. Cai. Methods for evaluation of retinal microvascular abnormalities associated with hypertension/sclerosis in the Atherosclerosis Risk in Communities Study. Ophthalmology, 106:2269-2280, 1999
7. F. E. Kruse, R. O. W. Burk, H. E. Völcker, G. Zinser, and U. Harbarth. Reproducibility of topographic measurements of the optic nerve head with laser tomographic scanning. Ophthalmology, 96:1320-1324, 1989.
8. L. Kubecka, J. Jan. Registration of Bimodal Retinal Images - improving modifications. In Proc. 26th Internat. Conf. IEEE-EMBS. 26th Annual International Conference of the IEEE Engineering in Medicine and Biology Society. San Francisco: IEEE, 2004, s. 1695 - 1 698.
9. D. Kucera. Segmentation of Multidimensional Image Data in Medicine. PhD thesis, TU, Brno, Czech Republic, 1996.
10. C. Y. Mardin and A. G. Jünemann. The diagnostic value of optic nerve imaging in early glaucoma. Current Opinion in Ophthalmology, 12:100-104, 2001.
11. G. Michelson and M. J. M. Groh. Screening models for glaucoma. Current Opinion in Ophthalmology, 12:105-111, 2001.
12. S. Miglior, E. Albe, M. Guareschi, L. Rossetti, and N. Orzalesi. Intraobserver and interobserver reproducibility in the evaluation of optic disc stereometric parameters by Heidelberg Retina Tomograph. Ophthalmology, 109:1072-1077, 2002.
13. F. S. Mikelberg, C. M. Parfitt, N. V. Swindale, S. L. Graham, S. M. Drance, and R. Gosine. Ability of the Heidelberg Retina Tomograph to detect early glaucomatous visual field loss. Journal of Glaucoma, 4:242-247, 1995.
14. I. Pál, H. Niemann, and G. Michelson. Experiment mit mehrschichtigen Perzeptron-Netzen zur Vorverarbeitung und Merkmalgewinnung auf den SLDF-Perfusionsbildern der Netzhaut. In H. Evers, G. Glombitza, T. Lehman, and H.-P. Meinzer, 1999. (Springer, Berlin, Heidelberg).
15. H. A. Quigley. Number of people with glaucoma worldwide. British Journal of Ophthalmology, 80:389-393, 1996.